

Enhancing CPT-Based Suction Caisson Penetration Design: Insights from Back-analysis of Large-Scale Field Installation Data

Stephen K. Suryasentana¹, Brendan F. O'Boyle², John Davidson³, Sarunas Bartkus⁴, Felix Schroeder⁵, Zefeng Zhou⁶

Affiliations

¹ Senior Lecturer, Department of Civil and Environmental Engineering, University of Strathclyde, 75 Montrose St, Glasgow G1 1XJ, UK.

² Geotechnical Engineer, SSE Renewables, 1 Waterloo St, Glasgow G2 6AY, UK.

³ Senior Geotechnical Engineer, Corio Generation, 33 Charterhouse St, London EC1M 6HA, UK.

⁴ Geotechnical Engineer, SSE Renewables, 1 Waterloo St, Glasgow G2 6AY, UK.

⁵ Senior Partner, Geotechnical Consulting Group LLP, Cromwell Road, London SW7 5BE, UK.

⁶ Senior Researcher, NGI - Norwegian Geotechnical Institute, Sandakerveien 140, 0484 Oslo, Norway.

Corresponding author information

Stephen Suryasentana

stephen.suryasentana@strath.ac.uk

Main text word count: 4987

Figures: 11

Tables: 7

Jul 30, 2024

Abstract

This paper presents a detailed back-analysis of large-scale field data from suction caisson installations in complex, layered soil conditions, enhancing the understanding of caisson installation interaction through a refined assessment of the parameters for Cone Penetration Test (CPT)-based installation calculation methods. Leveraging CPT and suction caisson installation data from a large database, this paper proposes a more nuanced CPT-based design approach tailored for such complex soil conditions. The findings highlight notable parameter differences between dilative and contractive soils, suggesting the necessity of treating these two groups distinctively. Through a comparative analysis with existing CPT-based methods, this research highlights areas where current practices align well with field realities and identifies areas where crucial adjustments are needed to enhance design accuracy. The paper also proposes a quantile-based approach for high estimate installation calculations, which demonstrates an effective balance between safety and excessive conservatism.

Keywords

Foundations, Soil-structure interaction, Back-analysis, Offshore

Introduction

The offshore wind energy industry is experiencing rapid growth, positioning itself as a pivotal element in the global shift towards renewable energy. The establishment of offshore wind farms necessitates foundations that are both reliable and economically viable to ensure the stability of structures and the reliable operation of wind turbines. Suction caisson foundations have emerged as a popular solution for offshore wind farms (OWA 2019; Bienen et al. 2018) in water depths ranging from about 40 to 60 meters. This preference is attributed to the benefits of the suction-aided installation technique, which offers a cost-effective and less noisy alternative to the conventional pile-driving methods used for monopile foundations. Despite its advantages, the suction-aided installation process faces significant uncertainties, particularly in complex, stratified soil conditions. While recent research has focused on improving design methodologies for the post-installation performance of suction caissons (e.g., Vulpe 2015; Foglia et al. 2015; Sturm 2017; Jalbi et al. 2018; Gelagoti et al. 2018; Efthymiou and Gazetas 2018; Skau et al. 2018, 2019; Antoniou et al. 2022; Suryasentana et al. 2017, 2018, 2022a, 2022b, 2023a, 2023b, 2024; Yin et al. 2020; Wu et al. 2022; Liu et al. 2023), there has been comparatively less attention on their installation performance (e.g., Klinkvort et al. 2019; Buckley et al. 2023; Huang et al. 2024). This underscores the need for improved design methodologies for caisson installation performance in complex interbedded layered soil conditions, particularly those validated by real-world field data (e.g., Byrne et al. 2020a, b).

This paper delves into the back-analysis of field installation data from suction caisson installations at the Seagreen offshore wind farm, a joint venture project between SSE Renewables and TotalEnergies. The main objective of this paper is to refine the Cone Penetration Test (CPT)-based approach for determining caisson penetration resistance

during suction-aided installation, thereby improving the reliability of the installation calculations for suction caisson foundations in challenging ground conditions.

The CPT is a widely used in-situ site investigation method that offers the convenience of continuous soil profiling, aiding in soil classification and foundation design (e.g., Suryasentana and Lehane 2014a, b, 2016; Buckley et al. 2023). CPT data is utilized within soil behavior type (SBT) classification systems, such as those developed by Robertson (1990, 2009) and Schneider et al. (2008), to classify soil according to its behavior characteristics. Traditionally, many of these SBT classification systems employ textural descriptors—like sand, gravelly sand, or clay—to categorize each SBT. Robertson (2016) introduced an updated CPT-based SBT classification that relies on descriptors reflective of the soil behavior for each category. This updated classification system categorizes soils based on their dilative or contractive properties, further identifying them as predominantly sand-like, clay-like, or somewhere in between (i.e., transitional soils). Dilative soils are characterized by an increase in volume under large strains, contrasting with contractive soils, which decrease in volume (Robertson, 2016).

There are two main types of design method (OWA, 2019) to determine the soil resistance to caisson penetration under suction-aided installation: mechanism-based (also known as ‘bearing capacity’-based) methods and CPT-based methods. Mechanism-based methods (e.g., Houlsby and Byrne 2005a,b) rely on standard geotechnical parameters obtained through in-situ or laboratory testing (e.g., undrained shear strength s_u), whereas CPT-based methods employ parameters derived from CPT (e.g., tip resistance q_c). This paper focuses on the CPT-based method, given the availability of CPT data corresponding to every caisson installation data. Various iterations of the CPT-based method exist (e.g., Andersen et al. 2008; Senders and Randolph 2009; DNV 2021), but they all share a common approach: the correlation of

local soil resistance to caisson penetration with local CPT tip resistance q_c , utilizing scale factors such as k_f and k_p . Here, k_f correlates to the frictional resistance along the caisson skirt, and k_p to the end-bearing resistance at the caisson tip. These factors are usually derived from the back-analysis of field data (e.g., Lunne and Kvalstad 1982; Anderson et al. 2008).

Research focusing on the back-analysis of field data concerning soil resistance to suction-aided penetration of caisson foundations is notably limited. DNV (2021) references the back-analysis study of Lunne and Kvalstad (1982), which provided estimates for the k_f and k_p factors based on field installation data from thirteen concrete gravity platforms in the North Sea, which are mainly installed in dense sands and stiff over-consolidated clays. Out of these, only seven platforms used steel skirts, and none of the installations involved suction pressure. Therefore, these factors do not account for the effect of suction-induced seepage on the caisson installation process. This is particularly important due to the significant impact seepage has on installation resistance in sand (Houlsby and Byrne 2005a). Anderson et al. (2008) performed a back-analysis of field-scale model tests involving seventeen suction caisson installations, primarily in sand. This analysis covered instances of suction-aided installation and resulted in estimates for the k_f and k_p factors that are consistent with the DNV (2021) guidelines. Klinkvort et al. (2019) expand on the method proposed by Andersen et al. (2008) to account for the effects of an impermeable layer beneath the caisson and an impermeable layer above the caisson tip. Further studies by Colliard and Wallerand (2008) and Frankenmolen et al. (2017) have expanded our knowledge on the k_f and k_p factors in normally consolidated clays and carbonate soils, respectively. Given that the existing installation methods are largely based on the back-analysis of a limited number of field installation data, the scarcity highlights the importance of conducting back-analyses on a larger database of field installation data

concerning real-world, suction-aided installations of caisson foundations. Such studies are critical for refining and validating the k_f and k_p factors, ultimately leading to more reliable suction caisson installation assessments.

The main contributions of this paper are as follows: First, it carries out a detailed back-analysis of an extensive dataset featuring 293 suction caisson installations at the Seagreen offshore wind farm project. This analysis aims to derive best estimates for the k_f and k_p factors that correspond to the measured field data. The dataset analyzed in this study is over ten times larger than those used in previous research, representing a substantial expansion in the volume of data examined. Second, it explores the variation of the k_f and k_p factors at different stages of the suction-aided installation process, which provides indirect insights into the influence of suction-induced seepage flow on these factors. Finally, it evaluates existing CPT-based design methods against field installation outcomes, distinguishing between scenarios where these methods demonstrate robust predictive capabilities and scenarios necessitating modifications for improved accuracy, which includes the proposal of a new design framework to address potential underestimation of the soil resistance to caisson penetration.

Case Study

The Seagreen offshore wind farm, located approximately 27km off the coast of Angus, Scotland, in the North Sea (see Figure 1a), stands as Scotland's largest wind farm to date. It comprises 114 wind turbine generators (WTGs), each boasting a capacity of 10 MW. These turbines are supported by jacket structures, each of which is anchored to the seabed by three suction caisson foundations. These caissons have outer diameters D ranging from 10.5m to 11.5m. The skirt wall thickness t is approximately $0.0052D$,

and the embedded skirt length L varies from $0.78D$ to $0.92D$. The installation of these caissons spanned across water depths varying from 42 meters to 59 meters LAT.

Ground conditions

The site for the Seagreen offshore wind farm exhibits a complex and variable stratigraphy, predominantly characterized by either mixed layers of sand, silts, and clays, or uniform layers of sand. The geological composition of the site primarily consists of Holocene and Pleistocene soils. A concise overview of these geological units is detailed in Table 1.

CPTs were conducted within the planned footprints of each suction caisson installation location. Figure 2 illustrates the variability of CPT-based normalized indices across the site, where $Q_{tn} = \frac{q_t - \sigma_{v0}}{\sigma'_{v0}}$ and $F_r = \left(\frac{f_s}{q_t - \sigma_{v0}} \right) \times 100 \%$, with q_t and f_s representing the tip resistance (corrected for pore water pressure effects) and sleeve friction from the CPT data, respectively. σ_{v0} and σ'_{v0} denote the current in-situ total and effective vertical stresses, respectively. The broad range between the 5th and 95th percentiles of the indices underscore the significant variability in soil conditions across the site.

The analysis of the CPT data, guided by the Robertson (2016) SBT classification system, discerns soil behaviors into seven categories based on the Q_{tn} and F_r values, as outlined in Table 2. The distribution of soil behavior types with depth across the site, as summarized in Figure 3, reveals that dilative sand is the predominant soil behavior at all depths, followed by dilative clay and transitional soil. Deeper layers frequently contain contractive clays, whereas contractive sand and transitional soils are primarily encountered at shallow depths.

Methodology

The primary objectives of installation design calculations for suction caisson foundations are twofold: Firstly, to estimate the caisson penetration behavior in scenarios where suction is not applied, effectively when only the self-weight of the caisson and its supporting structure are considered — this is referred to as ‘self-weight penetration’ (SWP). Secondly, to estimate the suction-aided caisson penetration response, which involves determining the suction pressures necessary to achieve the desired penetration depth. This step includes evaluating the predicted suction pressures against potential limitations arising from phenomena such as cavitation and structural buckling, ensuring that the design remains within safe operational thresholds.

The basic equation for suction caisson installation calculation is based on the following force equilibrium equation:

$$V' + s(A_{caisson}) = R_{soil} \quad (1)$$

where V' , $A_{caisson}$, s and R_{soil} are the submerged vertical load (considering buoyancy effects), internal plan area of the caisson lid, suction pressure applied (calculated as the difference between the pressure outside and inside the caisson), and total soil resistance to caisson penetration (which includes the soil resistance along the inner and outer walls of the caisson skirt, and at the tip of the caisson skirt).

This paper focuses on the CPT-based method recommended by DNV (2021), as follows:

$$V' + s(A_{caisson}) = A_{sk} \left(\int_0^h k_f(z) q_c(z) dz \right) + A_{tip} (k_p(h) q_c(h)) \quad (2)$$

where the right-hand side of Eq. 2 represents R_{soil} . z is depth below seabed, h is depth of the caisson tip below seabed, D_i is the inner caisson diameter, $A_{sk} = \pi(D + D_i)$ and

$A_{tip} = \frac{\pi}{4}(D^2 - D_i^2)$, as shown in Figure 1b. k_f and k_p are the factors for the frictional and end-bearing component of the soil resistance, respectively. The DNV suggested values for k_f and k_p are summarized in Table 3. For the purposes of this study, in the absence of DNV suggested factor values for transitional soils, the assumed factors for these soils are derived as the average of the factors provided for sand and clay. This approximation acknowledges the intermediate nature of transitional soils, positing that their behavior under caisson penetration might similarly lie between that of purely sandy or clayey soils. Moreover, as the DNV suggestions do not distinguish between dilative and contractive soils, the same suggested factors are assumed for both soil groups.

The aim of this paper is to conduct a detailed back-analysis to determine the best estimates of the k_f and k_p factors in Eq. 2 that best match the full-scale, field observations of the suction caisson installations. Notably, this analysis deviates from existing approaches by not solely relying on broad soil categories (e.g., clay, sand) as prescribed in Table 3. Instead, it adopts a more nuanced approach, aligning with the Robertson (2016) SBT classification system. This approach is adopted to investigate if substantial differences exist between dilative and contractive soils regarding the k_f and k_p factors.

To achieve these aims, the study compiled a dataset that matches the caisson installation data with proximate CPT data. The caisson installation data provides structural information such V' , $A_{caisson}$ and D , as well as measurements of the suction pressure s and the corresponding penetration depth. This dataset focuses exclusively on caisson installation under non-cyclic suction pressure. The assembled dataset encompasses data from 293 caisson installations, yielding approximately 123,000 data

points corresponding to the force equilibrium condition represented by Eq. 2. Note that there are no data points for sensitive contractive clay-like (SCC) soils.

The dataset is partitioned as follows: (i) 80% of the caisson installation locations are randomly selected to form the training dataset. This subset is used to back-analyze the k_f and k_p factors; (ii) the remaining 20% serve as the test dataset, used to evaluate the reliability of caisson installation calculations based on the back-analyzed factors. This approach allows for validation of the factors when applied to similar, but previously unseen, ground conditions. Figures 2 and 3 compare the CPT-based indices and the Robertson (2016) classifications for the training and test datasets, which indicate that the two datasets are broadly similar.

Figure 4a, which outlines the distribution of these data points from the training dataset across the various SBT categories, reveals a predominant representation of dilative soils, particularly dilative sand (SD). This distribution pattern aligns with observations from Figure 3a. To account for the different k_f and k_p factors pertaining to each SBT category, Eq. 2 can be rewritten as:

$$V' + s(A_{caisson}) = A_{sk} \left(\sum_{j \in C} k_f^j q_{sk}^j \right) + A_{tip} \left(\sum_{j \in C} k_p^j q_{tip}^j \right) \quad (3)$$

where C refers to the set of Robertson (2016) SBT categories i.e., {SD, TD, CD, SC, TC, CC, SCC}. k_f^j and k_p^j are the values of k_f and k_p for SBT category j . $q_{tip}^j = q_c(h)$ if the SBT category at depth h is j , else $q_{tip}^j = 0$. q_{sk}^j is the total q_c resistance along the caisson skirt till depth h for SBT category j , which is calculated as follows:

$$q_{sk}^j = \int_{z_1^{\text{top}}}^{z_1^{\text{bottom}}} q_c(z) dz + \dots + \int_{z_n^{\text{top}}}^{z_n^{\text{bottom}}} q_c(z) dz \quad (4)$$

where z_i^{top} and z_i^{bottom} refer to the top and bottom depth of the i th soil layer that has been classified as SBT category j . Note that only layers encountered from depth 0 to h

are considered in the integration i.e., $z_n^{\text{bottom}} \leq h$. If there is no soil layer of SBT category j encountered from depth 0 to h , then $q_{sk}^j = 0$.

To minimize the caisson dimensions from biasing the regression analysis when determining the best estimates for the k_f and k_p factors, the following stress-based form of Eq. 3 is used:

$$\frac{V'}{A_{\text{caisson}}} + s = \frac{A_{sk}}{A_{\text{caisson}}} \left(\sum_{j \in C} k_f^j q_{sk}^j \right) + \frac{A_{tip}}{A_{\text{caisson}}} \left(\sum_{j \in C} k_p^j q_{tip}^j \right) \quad (5)$$

For regression analysis, it is convenient to express Eq. 5 in vector form as follows:

$$\mathbf{a} \cdot \mathbf{x} = b \quad (6)$$

where \mathbf{a} and \mathbf{x} are both 14x1 vectors and b is a scalar. They are defined as:

$$\mathbf{a} = \left[\frac{A_{sk}}{A_{\text{caisson}}} q_{sk}^{SD}, \dots, \frac{A_{sk}}{A_{\text{caisson}}} q_{sk}^{SCC}, \frac{A_{tip}}{A_{\text{caisson}}} q_{tip}^{SD}, \dots, \frac{A_{tip}}{A_{\text{caisson}}} q_{tip}^{SCC} \right]^T \quad (7)$$

$$\mathbf{x} = \left[k_f^{SD}, \dots, k_f^{SCC}, k_p^{SD}, \dots, k_p^{SCC} \right]^T \quad (8)$$

$$b = \frac{V'}{A_{\text{caisson}}} + s \quad (9)$$

Here, \mathbf{x} represents the unknown k_f and k_p factors for the SBT categories.

The training dataset contains approximately 99,000 instances of Eq. 6, which can be collectively expressed in the following general matrix form:

$$\mathbf{A}\mathbf{x} = \mathbf{b} \quad (10)$$

where \mathbf{A} is a rectangular matrix whose rows are made up of \mathbf{a} from Eq. 7 pertaining to different installation locations and depths, while \mathbf{b} is a vector whose components is made up of b from Eq. 9 corresponding to those installation locations and depths.

As \mathbf{A} represents an overdetermined system of equations (i.e., there are more equations than unknowns), Eq. 10 does not have an exact solution and thus, the least squares

method is used to determine the best estimates for the k_f and k_p factors. However, ordinary least squares (OLS) solution may result in negative values for these factors, which are not physically meaningful given that these factors represent resistance and should inherently be non-negative. To address this issue, the current study employs the Non-Negative Least Squares (NNLS) technique, which is an extension of the OLS problem that adds a constraint: every element of the solution vector x must be greater than or equal to zero. The NNLS problem can be mathematically formulated as a convex optimization problem, as follows:

$$\begin{aligned} & \underset{x}{\text{minimize}} \quad \|Ax - b\|^2 & (11) \\ & \text{subject to} \quad x \geq \mathbf{0} \end{aligned}$$

The convex nature of the problem ensures that a globally optimal solution exists and can be efficiently found (Boyd and Vandenberghe, 2004). For the current study, the solution x to Eq. 10 is obtained using the algorithm proposed in Bro and De Jong (1997). If there are no negative components in x under OLS, then the NNLS solution will be similar to the OLS solution. In practical terms, any components in x that are negative under OLS are usually set to zero in the NNLS solution.

Using the solution x (i.e., the best estimates for the k_f and k_p factors), the best estimate for the stress-based soil resistance r_{soil}^{BE} can be calculated as:

$$r_{soil}^{BE} = \frac{A_{sk}}{A_{caisson}} \left(\sum_{j \in C} k_f^j q_{sk}^j \right) + \frac{A_{tip}}{A_{caisson}} \left(\sum_{j \in C} k_p^j q_{tip}^j \right) \quad (12)$$

For installation calculations, it is common practice to predict both ‘best estimate’ (BE) and ‘high estimate’ (HE) calculations. The HE calculation represents a conservative approach, essentially preparing for more challenging soil conditions than those typically anticipated. DNV (2021) suggests the use of the ‘Highest Expected’ factors in Table 3

to determine this HE calculation. The current paper, however, proposes an alternative quantile-based approach to determine the HE calculation:

$$r_{soil}^{HE} = r_{soil}^{BE} + \varepsilon_{HE} \quad (13)$$

where ε_{HE} is a high estimate (e.g., 95th) percentile of the residual error that defines the desired level of conservatism. The residual error ε is defined as follows:

$$\varepsilon = \frac{V'}{A_{caisson}} + s - r_{soil}^{BE} \quad (14)$$

The residual error quantifies the mismatch between the field measurements and the model calculations using the back-analyzed factors. The purpose of the quantile-based approach is to address potential underestimation by the back-analyzed model when compared to field measurements. This underestimation can occur because the model has a limited number of adjustable parameters and is calibrated to best match field measurements in a least-squares sense. Consequently, while the model aims to minimize the overall error, it may still underpredict some field measurements. The quantile-based approach compensates for this potential underestimation, ensuring that the HE calculation will meet or exceed the field measurements at a chosen target confidence level. For example, if the 95th percentile of the residual error is used for the HE calculation in Eq. 13, then there is only a 5% chance that the HE calculation is lower than the field measurement.

Bootstrapping

The bootstrap method (Efron 1979) is a powerful resampling technique for assessing the sensitivity of regression analysis results to changes in dataset composition. This approach involves generating numerous bootstrap samples from the original dataset by sampling with replacement, followed by the computation of regression solutions across these samples (Efron and Tibshirani 1994).

The current study generates 20,000 bootstrap samples by randomly sampling the caisson installations in the training dataset. Each bootstrap sample contains a random subset of these installations, meaning some installations may be omitted. This simulates the back-analysis outcomes if fewer caisson installations had been available. The best estimate for the k_f and k_p factors are determined for each bootstrap sample by solving the corresponding Eq. 11 problem. Through this process, the variability and reliability of the estimated parameters can be evaluated, offering insights into how the regression outcomes might vary with different subsets of the data. This will facilitate an assessment of whether additional caisson installation data collection might significantly alter the regression results.

Variation of factors during suction-aided installation in sand

During suction-assisted caisson installation in sand, the applied suction can induce changes in the soil properties which can influence the caisson penetration resistance as the installation progresses. The reduction in the caisson installation resistance is attributable to the induced seepage field and decreased effective stresses within the internal soil plug. While this physical phenomenon is understood qualitatively, precise quantitative analysis remains challenging due to the complex stress states involved.

This phenomenon, which is not captured in the DNV model (i.e., Eq. 2), was considered in the mechanism-based method (Houlsby and Byrne 2005a) and CPT-based method (e.g., Andersen et al. 2008; Senders and Randolph 2009) for sand. Senders and Randolph (2009) propose a model based on the following assumptions: (i) external friction along the caisson skirt remains constant regardless of applied suction; (ii) internal friction along the caisson skirt and tip resistance decrease linearly with the degree of mobilized critical suction s_{crit} , which is defined as the suction pressure level at which piping occurs. The model can be described as follows:

$$V' + s(A_{caisson}) = \pi D \left(\int_0^h k_f(z) q_c(z) dz \right) + \pi D_i \left(\int_0^h k_f(z) \left(1 - \frac{s}{s_{crit}} \right) q_c(z) dz \right) + A_{tip} \left(k_p(h) \left(1 - \frac{s}{s_{crit}} \right) q_c(h) \right) \quad (15)$$

where

$$s_{crit} = 1.32\gamma' D \left(\frac{L}{D} \right)^{0.75} \quad (16)$$

The application of the $\left(1 - \frac{s}{s_{crit}} \right)$ multiplier effectively reduces the k_f factor for internal friction and the k_p factor for tip resistance to zero when $\frac{s}{s_{crit}} = 1$.

Eq. 2 does not capture the effect of applied suction for caisson installations in sand. Thus, the current study investigates how the best estimates of the k_f and k_p factors for sand change as the applied suction increases. The analysis begins by creating a 'sand-only' dataset, extracted from the training dataset to include only caisson installation data from locations with uniform sand conditions. The resultant 'sand-only' dataset contains only caisson installations in dilative sand. Thereafter, multiple subsets of the 'sand-only' dataset are formed, each containing installation data up to progressively advanced stages of the suction-aided installation process. For each subset, a NNLS regression analysis is performed to determine the best estimates of the factors. By examining the variations in these factors, the study identifies how they change as applied suction increases.

Results

Table 4 shows the NNLS solutions for the best estimates of the k_f and k_p factors (rounded to two significant figures) across the Robertson (2016) SBT categories. A significant finding is the marked difference in these factors between dilative soils (SD, CD, TD) and contractive soils (SC, CC, TC). k_f^{SC} is approximately 100 times larger than k_f^{SD} , while k_f^{CC} and k_f^{CD} are broadly similar. Contractive soils exhibit significantly higher

k_p factors than their dilative counterparts. Notably, the k_f and k_p factors for both dilative and contractive transitional soils (TD, TC) are close to the average of the corresponding factors for sand and clay.

In comparison to the DNV suggested values in Table 3, the back-analyzed k_f factors for dilative soils are in very close agreement. However, the k_p factors for dilative soils diverges from the DNV suggested values, with k_p^{SD} being smaller, while k_p^{CD} is larger. For contractive soils, the k_f and k_p factors are much larger than the DNV suggested values, except for k_f^{CC} which is comparable.

Figures 5 and 6 show the histograms of the bootstrap estimates for the k_f and k_p factors as obtained from the NNLS solutions for the bootstrap samples. The best estimates for these factors obtained using the full dataset (as detailed in Table 4) are also included in these figures (as vertical dashed lines) for comparison. It is evident that these best estimates are very close to the modes of the histograms. The best estimates for k_f^{SD} and k_p^{SD} are slightly away from the modes but they are similar when comparing them to two significant figures. These results suggest that the dataset has reached a critical volume sufficient for deriving robust estimates, at least for the ground conditions encountered at the site. This robustness enhances confidence in the reliability of the back-analyzed factors and their resilience against dataset variability, thereby mitigating concerns about overfitting. Nevertheless, the variability of the factors for the contractive soils is greater than that for the dilative soils. One possible explanation for this is the much smaller volume of data for the former compared to the latter. Another possible explanation is that there are other effects contributing to the observed variability. These effects could include a changing relationship between skin friction and tip resistance with depth or latent relationships between resistance and

caisson geometry. These effects are masked by the modeling assumption that k_f and k_p factors remain constant regardless of depth or geometry. The current study's back-analysis is based on a narrow range of caisson geometries and is therefore most applicable to installations with similar dimensions. Future work could benefit from an expanded dataset that includes a wider variety of geometries, allowing for refined calibration of these factors and investigation of possible geometry-specific effects.

Figure 7 presents the best estimates of the k_f and k_p factors obtained for dilative sand using the subsets of the 'sand-only' dataset that corresponds to progressively advanced stages of the suction-aided installation process. These estimates highlight notable trends. The k_f factor at the end of SWP (i.e., before suction is applied) is almost double the corresponding value in Table 4. As the applied suction increases, the k_f factor initially increases slightly from 0.0022 to 0.0028 before gradually decreasing and stabilizing at 0.0011 (the value in Table 4). In contrast, the k_p factor at the end of SWP is almost half the corresponding value in Table 4. As the applied suction increases, the k_p factor initially decreases slightly from 0.062 before gradually increasing and stabilizing at 0.12 (the value in Table 4).

Figure 8 provides an overview of the accuracy of the caisson installation calculations for the training dataset using the DNV and back-analyzed factors. Figure 8a shows the histogram of the normalized residual errors (see Eq. 14) of the installation calculations using the best estimate k_f and k_p factors in Tables 3 and 4. The errors based on the back-analyzed factors are approximately normally distributed, while those based on the DNV factors have a left-skewed distribution. This indicates that the measured values are generally smaller than those predicted using the DNV factors. This observation is supported by Figure 8b, which shows the mean, 5th and 95th percentile for the residual

errors. Figure 8b also shows that the range between the 5th and 95th percentile for the DNV residual errors is much greater than that for the back-analyzed residual errors.

Figure 9 compares the installation calculations using the best estimate factors in Tables 3 and 4, across some varied ground conditions within the training dataset. The figure also shows the ground conditions of the installation locations, according to the Robertson (2016) SBT system. The colors of the SBT categories in Figure 9 are based on the same legend shown in Figure 3. Figure 9 presents the installation calculations in terms of normalized applied suction s/p_{atm} , which is defined as follows:

$$\frac{s}{p_{atm}} = \frac{r_{soil}}{p_{atm}} - \frac{V'}{A_{caisson}p_{atm}} \quad (17)$$

Figure 9a represents the base case with uniform dilative sand conditions. It shows that the installation calculations using the back-analyzed factors from Table 3 closely match the measured values. In contrast, the DNV calculations predict larger suction pressures than the measured values.

Figure 9b represents a location with dilative clay at shallower depths and primarily dilative sand below the SWP depth. The figure shows that the calculations using the back-analyzed factors underpredict the measured values at the shallower depths but match the measured values at the deeper depths. In contrast, the DNV calculations underpredict at the shallower depths and overpredict at the deeper depths.

Figures 9c and 9d illustrate complex cases with many interbedded layers below the SWP depth. In Figure 9c, the calculations using both the back-analyzed and DNV factors generally underpredict the measured values for most of the installation depth. In Figure 9d, the calculations using both the back-analyzed and DNV factors are generally

in line with the measured values, although the DNV calculations slightly underpredict the measured values in the dilative clay layers.

Beside the calculations using the best estimate factors in Tables 3 and 4, Figure 9 also includes the HE calculations, where the Highest Expected factors in Table 3 are used for the DNV HE calculations. Table 5 presents various percentile values derived from the histogram of residual errors in the back-analyzed calculations, as displayed in Figure 8a. These values are used for the proposed quantile-based HE calculation approach (i.e., Eq. 13). In Figure 9, the 95th percentile of the residual errors (i.e., Eq. 13, with $\varepsilon_{HE} = 1.14p_{atm}$ from Table 5) is employed for the back-analyzed HE calculations as an example. Figure 9 shows that the back-analyzed HE calculations is greater than the measured values for most depths across all locations. In contrast, the DNV HE calculations can be overly conservative (see Figures 9a and 9b).

To evaluate the reliability of the back-analyzed factors for caisson installation calculations in new, unseen data, they are applied to the test dataset. Figure 10 provides an overview of the accuracy of the caisson installation calculations for the test dataset using the DNV and back-analyzed factors. A comparison of Figure 8 and 10 demonstrates that the accuracy of calculations using the back-analyzed factors is consistent between the test and training datasets. The residual error skew and the range between the 5th and 95th percentiles are similar in both cases. This consistency confirms the reliability and applicability of the back-analyzed factors in new locations with comparable ground conditions. Additionally, Figure 11 shows the caisson installation calculations for some locations in the test dataset. Figure 11a represents the base case with uniform dilative sand conditions, while Figure 11b represents a location with dilative clay and transitional soils in the shallower depths but mainly dilative sand below the SWP depth. These figures illustrate that, under primarily dilative

sand conditions, the calculations using the back-analyzed factors from Table 4 closely match the measured values, whereas the DNV calculations are generally more conservative.

Figure 11c represents a location with dilative sand at shallower depths and mainly dilative clay below the SWP depth. The figure shows that the calculations using both the back-analyzed and DNV factors tend to underpredict the measured values for most of the installation depth. Figure 11d represents a complex case with many interbedded layers, where a significant portion of the ground conditions below the SWP depth consists of contractive clay. The figure demonstrates that at shallower depths, calculations based on the back-analyzed factors underestimate the measured values but align more closely at greater depths. In contrast, the DNV calculations consistently underestimate the measured values throughout the entire installation depth.

Regarding HE calculations, Figure 11 indicates that HE calculations using the back-analyzed factors generally exceed the measured values for most depths across all locations. On the other hand, the DNV HE calculations are either overly conservative (as shown in Figures 11a and 11b) or insufficiently conservative (as shown in Figure 11d).

Discussion

The results reveal a notably distinction between the k_f and k_p factors for dilative versus contractive soils. Specifically, contractive soils exhibit significantly higher factors than dilative soils, suggesting that using the same factors for dilative and contractive soils may not be appropriate. The higher k_p factor for contractive sand aligns with the recommendation of Senders and Randolph (2009), who suggested that the k_p factor

for loose sand should be higher than that of dense sand. However, it is important to acknowledge that the current study includes significantly less data on contractive soils compared to dilative soils. Nevertheless, the installation data in contractive soils still encompasses a total penetration depth of approximately 30m, which provides a substantial basis for preliminary analysis. Future research with a larger dataset on contractive soils would help to confirm these findings more conclusively.

The close alignment of the back-analyzed k_f factors for dilative soils with the DNV suggested values affirms the reliability of the DNV values. The back-analyzed k_f and k_p factors for dilative transitional soils also agree with the simplistic assumption of the values being the average of the corresponding sand and clay factors. However, discrepancies in the k_p factors highlight areas for potential adjustment. The DNV suggested value for k_p^{SD} may be too high, while its k_p^{CD} suggested value may not be high enough. The implications of the overly high k_p^{SD} is evident in Figures 9a and 9b, which illustrate the over-conservatism of the DNV calculations for locations predominantly composed of dilative sand, despite the DNV k_f^{SD} factor aligning closely with the back-analyzed value. On the other hand, the implications of the too low k_p^{CD} is evident in Figure 9d, which shows that the DNV installation calculations underestimate in layers of dilative clay, despite the DNV k_f^{CD} factor aligning closely with the back-analyzed value.

Figure 7 hints at the changing soil-caisson interaction during installation. The reduction of the k_f factor for dilative sand with increasing applied suction likely stems from the influence of seepage flow due to suction, which lowers the effective stress in the sand and, consequently, its resistance to caisson penetration. This is consistent with the findings of previous research (e.g., Senders and Randolph 2009). This suggests that

the best estimates of the back-analyzed k_f factors in Table 4 already represent conservative lower-bound values that account for the effect of suction. However, it is noted that the observed increase in the k_p factor in Figure 7b is unexpected, as Eq. 15 suggests that the k_p factor should decrease as applied suction increases. The reason for this is uncertain. It could be a modeling artifact of the k_p and k_f indirect estimation procedure, or it might represent a physical phenomenon that previous experimental studies did not capture. Further research is needed to clarify the underlying causes.

Figure 8b and 10b show that the DNV installation calculations are considerably more conservative than the actual measurements. Additionally, the broader range between the 5th and 95th percentiles of the error histograms for the DNV installation calculations points to a higher likelihood of extreme prediction errors across various ground conditions. This contrasts with the narrower error range for the back-analyzed installation calculations, which implies that using the back-analyzed factors in Table 4 provides potentially more robust and consistent performance, with fewer instances of extreme prediction errors. Furthermore, the similarity between the residuals errors of the calculations for the training and test dataset (compare Figures 8 and 10) provides more confidence in the reliability of the back-analyzed factors listed in Table 4. This reliability suggests that these factors can be effectively applied to ground conditions similar to those investigated in this study. This assertion is supported by the observation of similar Q_{tn} and F_r ranges in the training and test datasets, as depicted in Figure 2.

Figures 9c and 11c reveal a significant discrepancy between the back-analyzed model calculations and the field-measured data. This discrepancy arises because the model is based on a limited set of adjustable parameters (i.e., the k_f and k_p factors), which restricts its ability to match all field data precisely. Consequently, some model

predictions may under- or overestimate the observed values, as reflected in Figure 8. The model parameters were optimized to best fit the field data using a least-squares error approach, which inherently introduces some degree of mismatch. To address potential underestimations of soil resistance during installation, which are generally more critical than overestimations, this paper has proposed the quantile-based approach for HE calculations (Eq. 13). Another possible reason for this discrepancy could be lateral variation in soil conditions within the caisson footprint, which are not captured by the representative CPT data.

Figures 9 and 11 illustrate that the proposed quantile-based approach for HE calculations effectively addresses potential underestimations using the best estimate factors in Table 4, without being overly conservative. This approach compares well against the DNV approach to HE calculations, which can result in either extreme conservativeness (see Figures 9a, 9b, 11a and 11b) or insufficiency (see Figure 11d). Although this paper employs the 95th percentile of the residual errors for the HE calculations, other percentile values in Table 5 may be used to determine the HE calculations at the desired level of conservatism. Therefore, the quantile-based approach provides a balanced and pragmatic solution to accommodate significant deviations from anticipated outcomes during caisson installation, especially in ground conditions similar to those in the study.

This study has some limitations. The failure mechanism of soil at the skirt tip differs between SWP and suction-aided penetration, which would affect the penetration resistance and change the k_p factors. In the current study, the proposed CPT-based model does not explicitly account for this difference in failure mechanisms. Instead, for simplicity, it assumes identical k_p factors for all stages of penetration, similar to existing CPT-based installation design methods (e.g., DNV 2021). Although this idealization

may introduce some inaccuracy in SWP calculations, Figures 9 and 11 suggest that the resultant SWP calculations are reasonable. Another limitation of the current study is that previous research (e.g., Klinkvort et al. 2019) has shown that when a caisson skirt penetrates from a sand layer into a clay layer, suction-induced seepage flow may diminish, which would change the k_f and k_p factors in the sand layer. However, the current study does not quantify changes in the k_f and k_p factors under varying seepage flow conditions during soil layer transitions, mainly due to the complexity of the soil layering configurations (e.g., see Figure 9c). Furthermore, for ease of application, the proposed model assumes that these factors remain constant for each soil type, regardless of seepage flow conditions, aligning with the DNV (2021) CPT-based design method. Nevertheless, the back-analysis effectively accounts for different seepage flow conditions as it determines the constant k_f and k_p factors that best match the field observations across the range of seepage flow conditions encountered in different soil layer configurations during installation. However, it is acknowledged that a more detailed model that incorporates seepage flow-dependent k_f and k_p factors, as in the model proposed by Klinkvort et al. (2019), could provide more accurate estimates, presenting an area for future research.

Conclusion

This paper presents a detailed back-analysis of field data from suction caisson installations at a site with complex, multi-layered soil conditions. It refines the estimates of the k_f and k_p factors for a CPT-based suction caisson installation calculation method, using a nuanced soil classification system that differentiates between dilative and contractive soil behaviors as suggested by Robertson (2016). The study confirms the reliability of DNV's suggested values for the k_f factors for dilative soils but suggests that the DNV k_p factor for dilative sand may be too high. The findings highlight

significant differences in the back-analyzed k_f and k_p factors for dilative versus contractive soils and reveal the variable nature of the factors for dilative sand during different stages of the suction-aided installation phase.

To address potential underestimations using the back-analyzed factors, a quantile-based approach for high estimate installation calculations is proposed. This approach ensures safety without excessive conservatism. Overall, the insights from this research contribute to the development of more precise and effective design strategies for suction caisson installations, especially in soil conditions similar to those examined in this study.

Data Availability Statement

Some or all models, or code that support the findings of this study are available from the corresponding author upon reasonable request. The data used during the study are proprietary or confidential in nature.

Acknowledgments

The first author would like to thank EPSRC Supergen ORE Hub for supporting this work through the Flexible Funding scheme (FFF2023-1009). Additionally, the first author would like to thank SSE Renewables and TotalEnergies for providing the necessary data for this work.

List of notation

V'	submerged vertical load
$A_{caisson}$	internal plan area of the caisson lid
R_{soil}	total soil resistance to caisson penetration
s	applied suction pressure
p_{atm}	atmospheric pressure
r_{soil}	R_{soil} normalized by $A_{caisson}$
k_f	factor for soil resistance along caisson skirt
k_p	factor for soil resistance at caisson skirt tip
k_f^{SD}	k_f factor for dilative sand
k_f^{CD}	k_f factor for dilative clay
k_f^{TD}	k_f factor for dilative transitional soil
k_f^{SC}	k_f factor for contractive sand
k_f^{CC}	k_f factor for contractive clay
k_f^{TC}	k_f factor for contractive transitional soil
k_p^{SD}	k_p factor for dilative sand
k_p^{CD}	k_p factor for dilative clay
k_p^{TD}	k_p factor for dilative transitional soil
k_p^{SC}	k_p factor for contractive sand
k_p^{CC}	k_p factor for contractive clay
k_p^{TC}	k_p factor for contractive transitional soil
ε	residual error in caisson installation calculations
D	caisson outer diameter
D_i	caisson inner diameter
L	caisson skirt length
z	depth below seabed
h	depth of the caisson tip below seabed
q_c	CPT tip resistance
f_s	CPT sleeve friction
Q_{tn}	normalized CPT tip resistance
F_r	normalized CPT sleeve friction

References

- Andersen, K. H., Jostad, H. P., and Dyvik, R. (2008). Penetration resistance of offshore skirted foundations and anchors in dense sand. *Journal of geotechnical and geoenvironmental engineering*, 134(1), 106-116.
- Antoniou, M., Kourkoulis, R., Gelagoti, F., and Anastasopoulos, I. (2022). Simplified method for performance-based seismic design of suction caissons supporting jacket offshore wind turbines. *Soil Dynamics and Earthquake Engineering*, 155, 107169.
- Bienen, B., Klinkvort, R. T., O'loughlin, C. D., Zhu, F., and Byrne, B. W. (2018). Suction caissons in dense sand, part I: installation, limiting capacity and drainage. *Géotechnique*, 68(11), 937-952.
- Boyd, S.P. and Vandenberghe, L. (2004). *Convex optimization*. Cambridge university press.
- Bro, R., and De Jong, S. (1997). A fast non-negativity-constrained least squares algorithm. *Journal of Chemometrics: A Journal of the Chemometrics Society*, 11(5), 393-401.
- Buckley, R., Chen, Y. M., Sheil, B., Suryasentana, S., Xu, D., Doherty, J., and Randolph, M. (2023). Bayesian optimization for CPT-based prediction of impact pile drivability. *Journal of Geotechnical and Geoenvironmental Engineering*, 149(11), 04023100.
- Byrne, B.W., McAdam, R.A., Burd, H.J., Beuckelaers, W.J., Gavin, K.G., Houlsby, G.T., Igoe, D.J., Jardine, R.J., Martin, C.M., Muir Wood, A. and Potts, D.M., (2020a). Monotonic laterally loaded pile testing in a stiff glacial clay till at Cowden. *Géotechnique*, 70(11), 970-985.
- Byrne, B.W., Aghakouchak, A., Buckley, R.M., Burd, H.J., Gengenbach, J., Houlsby, G.T., McAdam, R.A., Martin, C.M., Schranz, F., Sheil, B.B. and Suryasentana, S.K., (2020b). PICASO: Cyclic lateral loading of offshore wind turbine monopiles. In

- Frontiers in Offshore Geotechnics IV: Proceedings of the 4th International Symposium on Frontiers in Offshore Geotechnics (ISFOG 2021).
- Colliard, D., and Wallerand, R. (2008). Design and installation of suction piles in West Africa deepwaters. In Proceedings of the Second British Geotechnical Association International Conference on Foundations (ICOF 2008) (Vol. 1, pp. 825-836).
- DNV (2021). DNV-RP-C212: Offshore soil mechanics and geotechnical engineering. Oslo, Norway.
- Efron, B. (1992). Bootstrap methods: another look at the jackknife. In Breakthroughs in statistics: Methodology and distribution (pp. 569-593). New York, NY: Springer New York.
- Efron, B., and Tibshirani, R. J. (1994). An introduction to the bootstrap. Chapman and Hall/CRC.
- Efthymiou, G. and Gazetas, G. (2018), Elastic Stiffnesses of a Rigid Suction Caisson and Its Cylindrical Sidewall Shell, *Journal of Geotechnical and Geoenvironmental Engineering* 145 (2), 06018014.
- Frankenmolen, S. F., Erbrich, C. T., and Fearon, R. E. (2017). Successful installation of large suction caissons and driven piles in carbonate soils. In Offshore Site Investigation Geotechnics 8th International Conference Proceeding (Vol. 539, No. 548, pp. 539-548). Society for Underwater Technology.
- Foglia, A., Gottardi, G., Govoni, L., and Ibsen, L. B. (2015). Modelling the drained response of bucket foundations for offshore wind turbines under general monotonic and cyclic loading. *Applied Ocean Research*, 52, 80-91.
- Gelagoti, F., Georgiou, I., Kourkoulis, R., and Gazetas, G. (2018). Nonlinear lateral stiffness and bearing capacity of suction caissons for offshore wind-turbines. *Ocean Engineering*, 170, 445-465.

- Houlsby, G. T., and Byrne, B. W. (2005a). Design procedures for installation of suction caissons in sand. *Proceedings of the Institution of Civil Engineers-Geotechnical Engineering*, 158(3), 135-144.
- Houlsby, G. T., and Byrne, B. W. (2005b). Design procedures for installation of suction caissons in clay and other materials. *Proceedings of the Institution of Civil Engineers-Geotechnical Engineering*, 158(2), 75-82.
- Huang, Z., Shi, L., Zhou, Z., and Cai, Y. (2024). Analytical solution for suction-induced seepage flow during suction bucket installation in multilayered soil with anisotropic permeability. *Computers and Geotechnics*, 171, 106393.
- Jalbi, S., Shadlou, M., and Bhattacharya, S. (2018). Impedance functions for rigid skirted caissons supporting offshore wind turbines. *Ocean Engineering*, 150, 21-35.
- Klinkvort, R. T., Sturm, H., and Andersen, K. H. (2019). Penetration model for installation of skirted foundations in layered soils. *Journal of Geotechnical and Geoenvironmental Engineering*, 145(10), 04019085.
- Liu, T., Zhang, Y., and Meng, Q. (2023). Numerical investigation and design of suction caisson for on-bottom pipelines under combined VHMT loading in normal consolidated clay. *Ocean Engineering*, 274, 113997.
- Lunne, T., and Kvalstad, T. (1982). *Analysis of Full-scale Measurements on Gravity Platforms: Final Report: Foundation Performance During Installation and Operation of North Sea Concrete Gravity Platforms*. Norwegian Geotechnical Institute.
- OWA (2019). *Suction Installed Caisson Foundations for Offshore Wind: Design Guidelines*. Carbon Trust.
- Robertson, P. K. (1990). Soil classification using the cone penetration test. *Canadian Geotechnical Journal*, 27(1), 151-158.
- Robertson, P. K. (2009). Interpretation of cone penetration tests—a unified approach. *Canadian Geotechnical Journal*, 46(11), 1337-1355.

- Robertson, P. K. (2016). Cone penetration test (CPT)-based soil behaviour type (SBT) classification system—an update. *Canadian Geotechnical Journal*, 53(12), 1910-1927.
- Schneider, J. A., Randolph, M. F., Mayne, P. W., and Ramsey, N. R. (2008). Analysis of factors influencing soil classification using normalized piezocone tip resistance and pore pressure parameters. *Journal of geotechnical and geoenvironmental engineering*, 134(11), 1569-1586.
- Senders, M., and Randolph, M. F. (2009). CPT-based method for the installation of suction caissons in sand. *Journal of geotechnical and geoenvironmental engineering*, 135(1), 14-25.
- Skau K. S., Grimstad G., Page A. M., Eiksund G. R. and Jostad H. P. (2018). A macro-element for integrated time domain analyses representing bucket foundations for offshore wind turbines. *Marine Structures*, 59, 158–78.
- Skau K. S., Jostad H. P., Eiksund G., Sturm H. P. (2019) Modelling of soil-structure-interaction for flexible caissons for offshore wind turbines. *Ocean Engineering*, 171, 273–85.
- Sturm, H. (2017). Design aspects of suction caissons for offshore wind turbine foundations. In *Unearth the Future, Connect beyond*. Proceedings of the 19th International Conference on Soil Mechanics and Geotechnical Engineering.
- Suryasentana, S. K., and Lehane, B. M. (2014a). Numerical derivation of CPT-based p - y curves for piles in sand. *Géotechnique*, 64(3), 186-194.
- Suryasentana, S. K., and Lehane, B. M. (2014b). Verification of numerically derived CPT based py curves for piles in sand. In *Proceedings of 3rd International Symposium on Cone Penetration Testing* (pp. 3-29). Las Vegas, Nevada USA.
- Suryasentana, S. K., and Lehane, B. M. (2016). Updated CPT-based p - y formulation for laterally loaded piles in cohesionless soil under static loading. *Géotechnique*, 66(6), 445-453.

- Suryasentana, S. K., Byrne, B. W., Burd, H. J., and Shonberg, A. (2017). Simplified model for the stiffness of suction caisson foundations under 6DoF loading. In Proceedings of SUT OSIG 8th International Conference, London, UK.
- Suryasentana, S. K., Byrne, B. W., Burd, H. J., and Shonberg, A. (2018). An elastoplastic 1D Winkler model for suction caisson foundations under combined loading. Numerical Methods in Geotechnical Engineering IX, 973-980. CRC Press.
- Suryasentana, S. K., Burd, H. J., Byrne, B. W., and Shonberg, A. (2022a). A Winkler model for suction caisson foundations in homogeneous and non-homogeneous linear elastic soil. *Géotechnique*, 7(5), 407-423.
- Suryasentana, S. K., and Mayne, P. W. (2022b). Simplified method for the lateral, rotational, and torsional static stiffness of circular footings on a nonhomogeneous elastic half-space based on a work-equivalent framework. *Journal of Geotechnical and Geoenvironmental Engineering*, 148(2), 04021182.
- Suryasentana, S. K., Burd, H. J., Byrne, B. W., and Shonberg, A. (2023a). Modulus weighting method for stiffness estimations of suction caissons in layered soils. *Géotechnique Letters*, 13(2), 1-8.
- Suryasentana, S. K., Burd, H. J., Byrne, B. W., and Shonberg, A. (2023b). Small-strain, non-linear elastic Winkler model for uniaxial loading of suction caisson foundations. *Géotechnique Letters*, 1-26.
- Suryasentana, S. K., Sheil, B. B., and Stuyts, B. (2024). Multifidelity Data Fusion for the Estimation of Static Stiffness of Suction Caisson Foundations in Layered Soil. *Journal of Geotechnical and Geoenvironmental Engineering*, 150(8), 04024066.
- Vulpe, C. (2015). Design method for the undrained capacity of skirted circular foundations under combined loading: effect of deformable soil plug. *Géotechnique*, 65(8), 669-683.

Wu, Y., Yang, Q., Li, D., and Zhang, Y. (2022). Limit equilibrium solutions to anti-overturning bearing capacity of suction caissons in uniform and linearly increasing strength clays. *Canadian Geotechnical Journal*, 59(2), 304-313.

Yin, Z. Y., Teng, J. C., Li, Z., and Zheng, Y. Y. (2020). Modelling of suction bucket foundation in clay: From finite element analyses to macro-elements. *Ocean Engineering*, 210, 107577.

Table 1. Main geological units encountered at the site.

Geological Units	Description
Holocene marine sands	Sand with occasional gravel or silts.
Forth Formation (Pre-Holocene and Early Holocene deposits)	Soft clays, silts and sand with some organic content.
Marr Bank and Wee Bankie Formations	Poorly to well sorted fine-grained sand, with layers of silts, gravels and clays

Table 2. Soil behavior type categories according to Robertson (2016).

Symbol	Description
SD	Sand-like - Dilative
TD	Transitional - Dilative
CD	Clay-like - Dilative
SC	Sand-like - Contractive
TC	Transitional - Contractive
CC	Clay-like - Contractive
SCC	Clay-like - Contractive - Sensitive

 Table 3. DNV (2021) suggested values for the k_f and k_p factors for clay and sand.

Soil type	Best Estimate		Highest Expected	
	k_p	k_f	k_p	k_f
Clay	0.4	0.03	0.6	0.05
Sand	0.3	0.001	0.6	0.003

 Table 4. Best estimate of k_f and k_p factors obtained using the full training dataset.

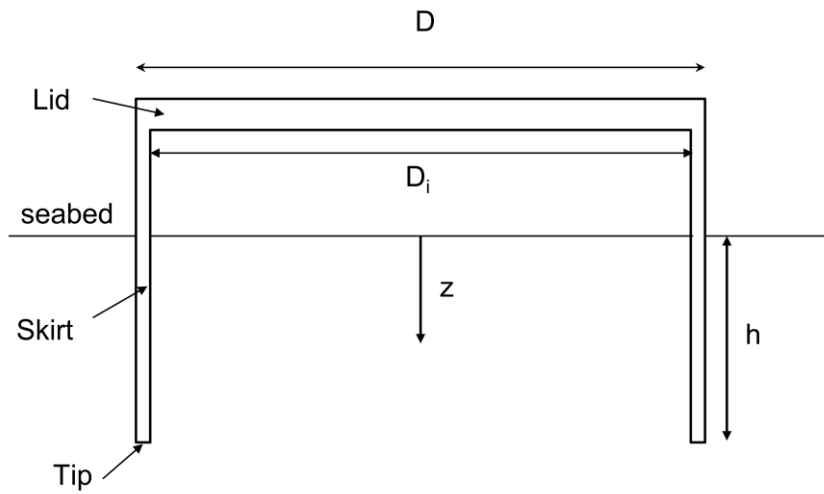
Soil type	Soil behavior type	Back-analyzed (Best Estimate)	
		k_p	k_f
Sand	SD	0.12	0.0011
Clay	CD	0.66	0.028
Transitional	TD	0.47	0.018
Sand	SC	1.1	0.13
Clay	CC	4.6	0.019
Transitional	TC	2.5	0.074

Table 5. Percentile values for the histogram of the residual errors of the back-analyzed calculations shown in Figure 8a.

Percentile	ε/p_{atm}
90 th	0.88
95 th	1.14
99 th	1.66
100 th	2.96



(a)



(b)

Figure 1. (a) Seagreen wind farm location, off the east coast of Scotland (b) Schematic diagram of a suction caisson installation

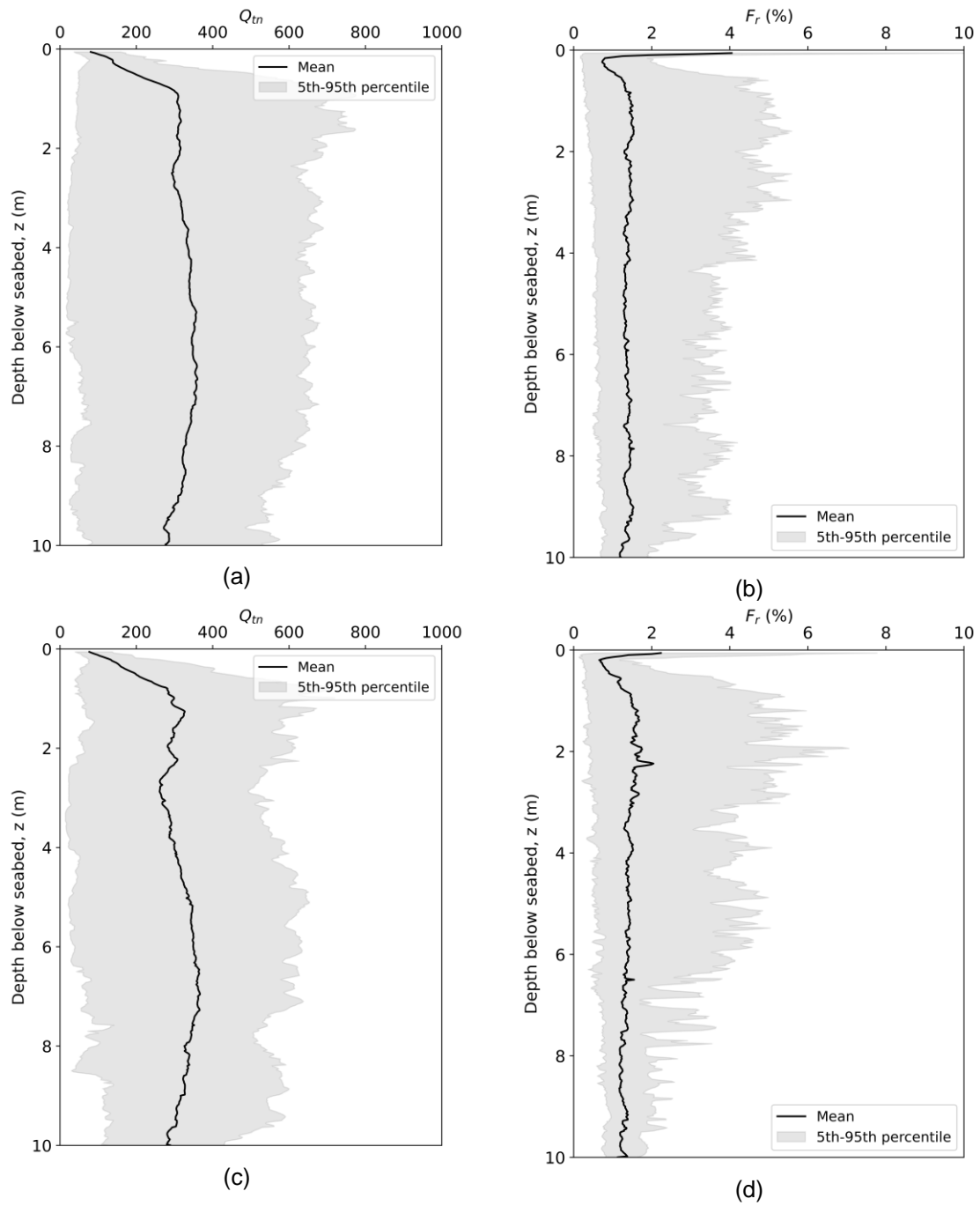
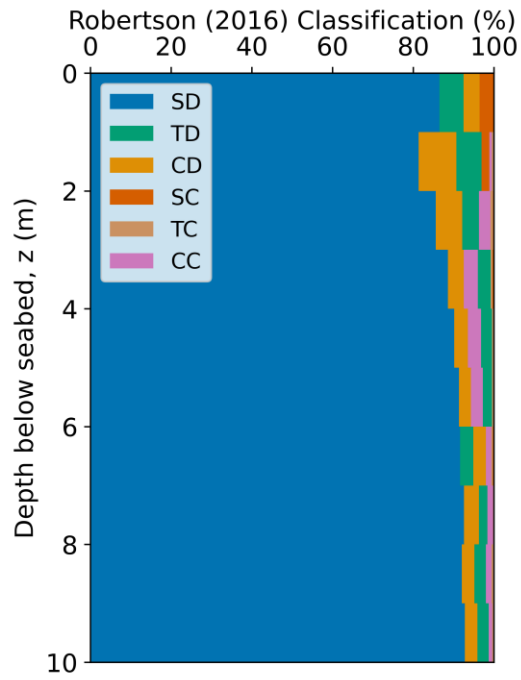
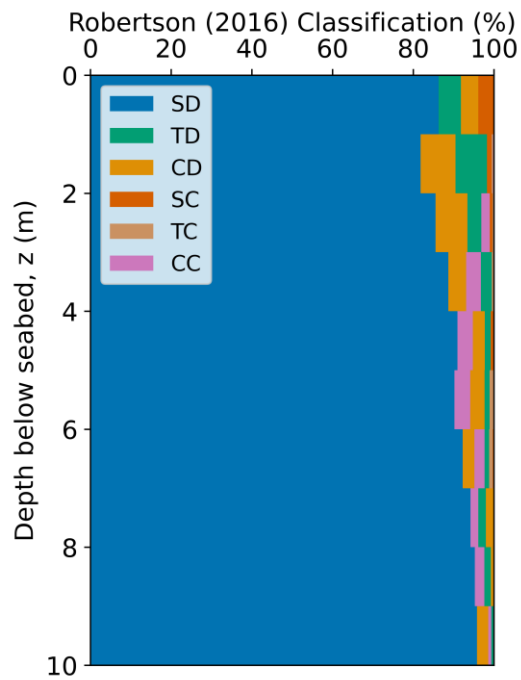


Figure 2. Depth profiles of the CPT-based indices, Q_{tn} and F_r , for the CPT data in the: (a)-(b) training dataset; (c)-(d) test dataset. The mean profile, together with the 5th to 95th percentile interval, is shown here.



(a)



(b)

Figure 3. Distribution of the Robertson (2016) classification for every 1m depth interval for the CPT data in the: (a) training dataset; (b) test dataset

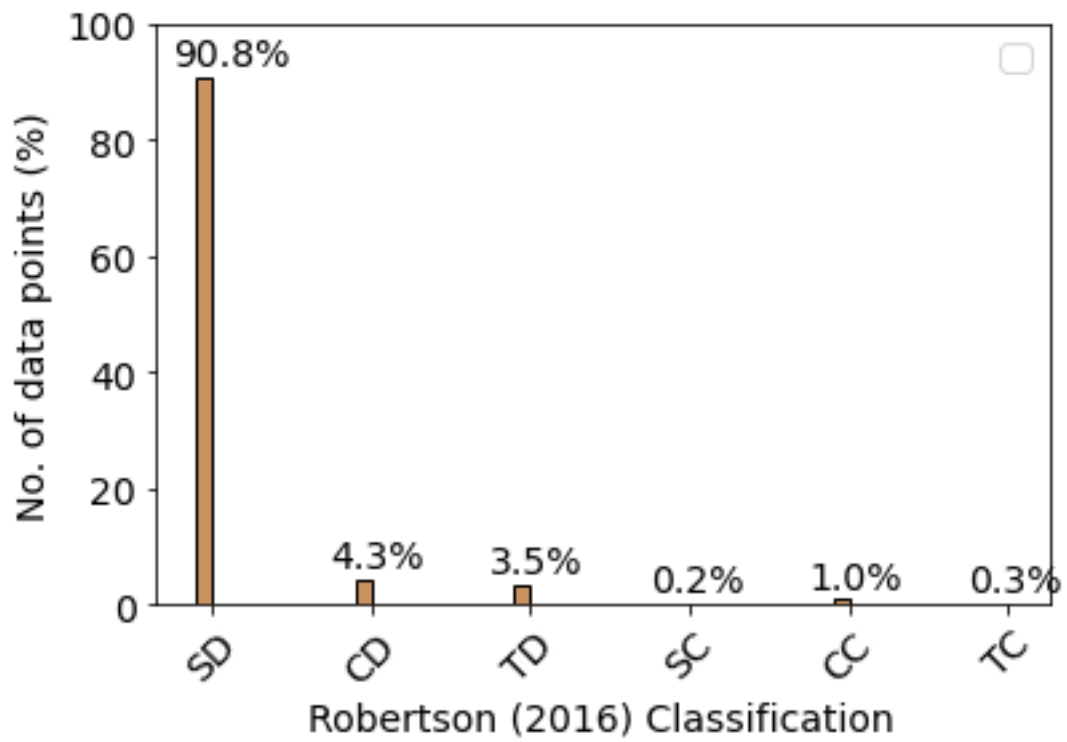


Figure 4. Distribution of data points for each Robertson (2016) SBT category for the full training dataset

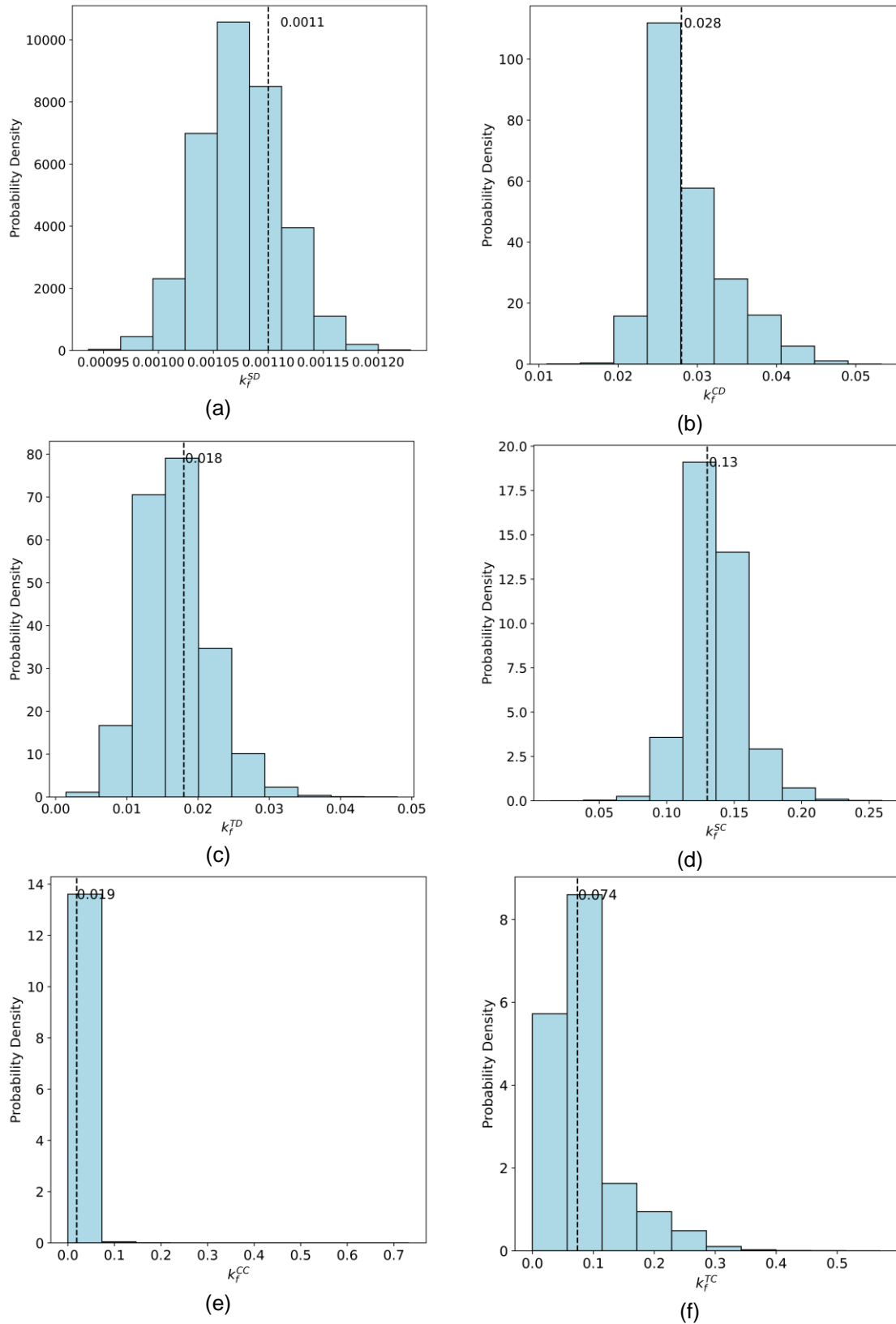


Figure 5. Histograms of the bootstrap estimates for the k_f factors.

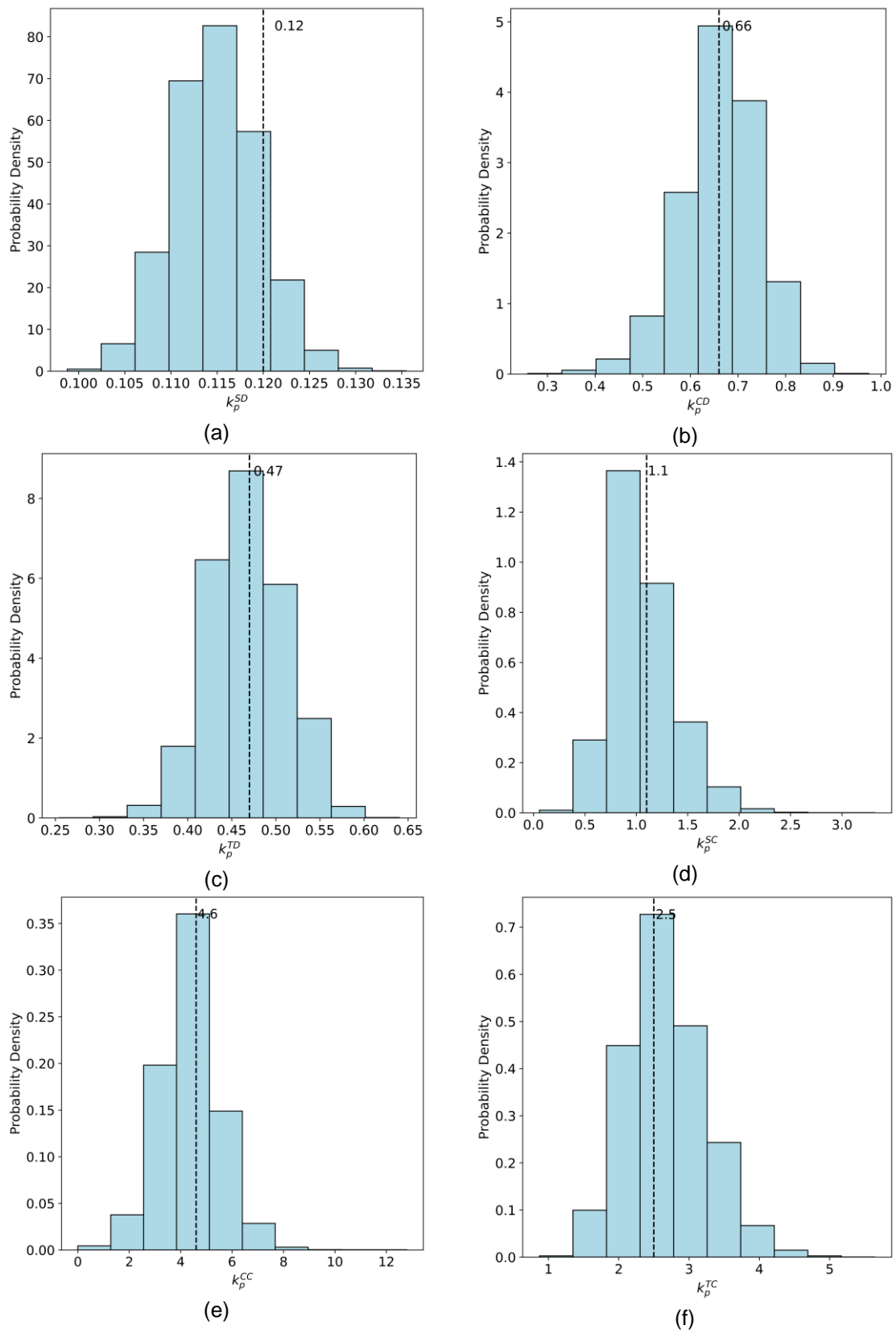
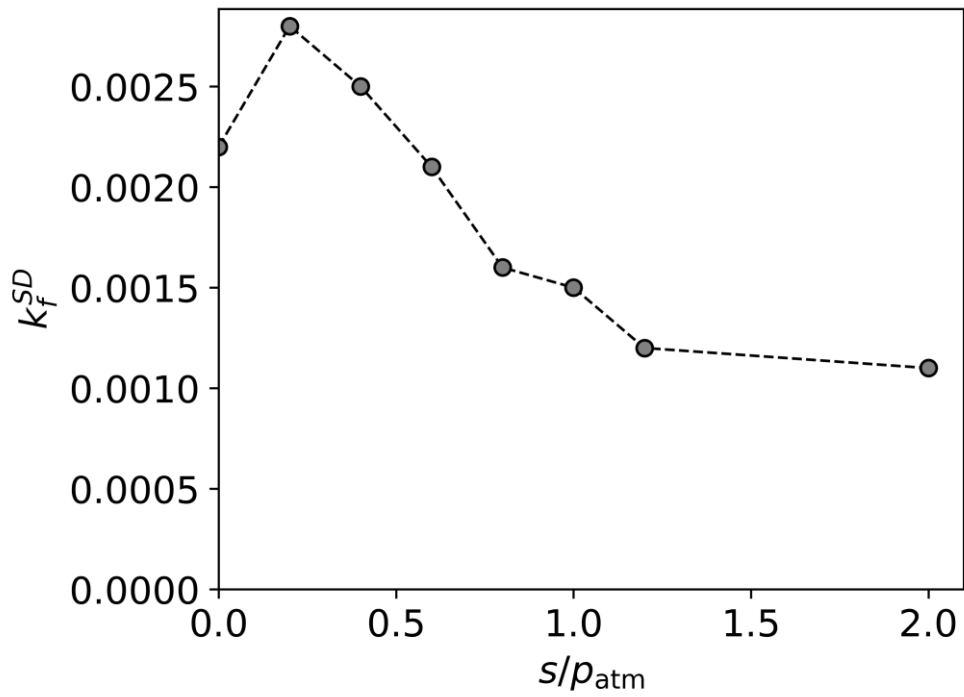
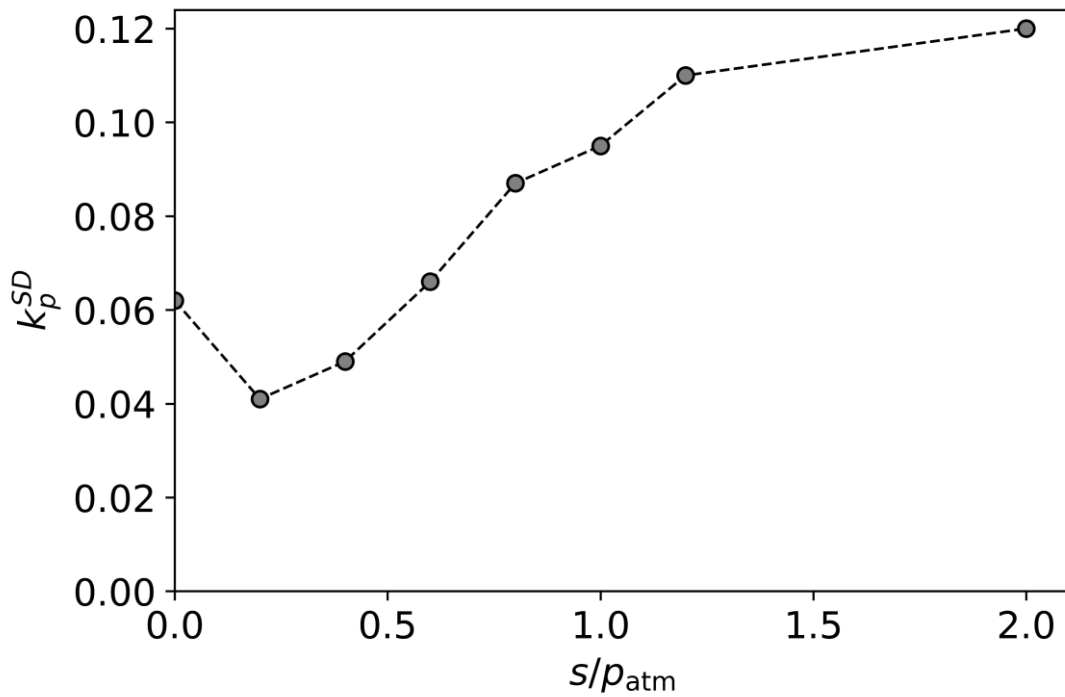


Figure 6. Histograms of the bootstrap estimates for the k_p factors.



(a)



(b)

Figure 7. Changes in the best estimates for the (a) k_f factor, and (b) k_p factor for caisson installations in dilative sand (SD) as the applied suction increases.

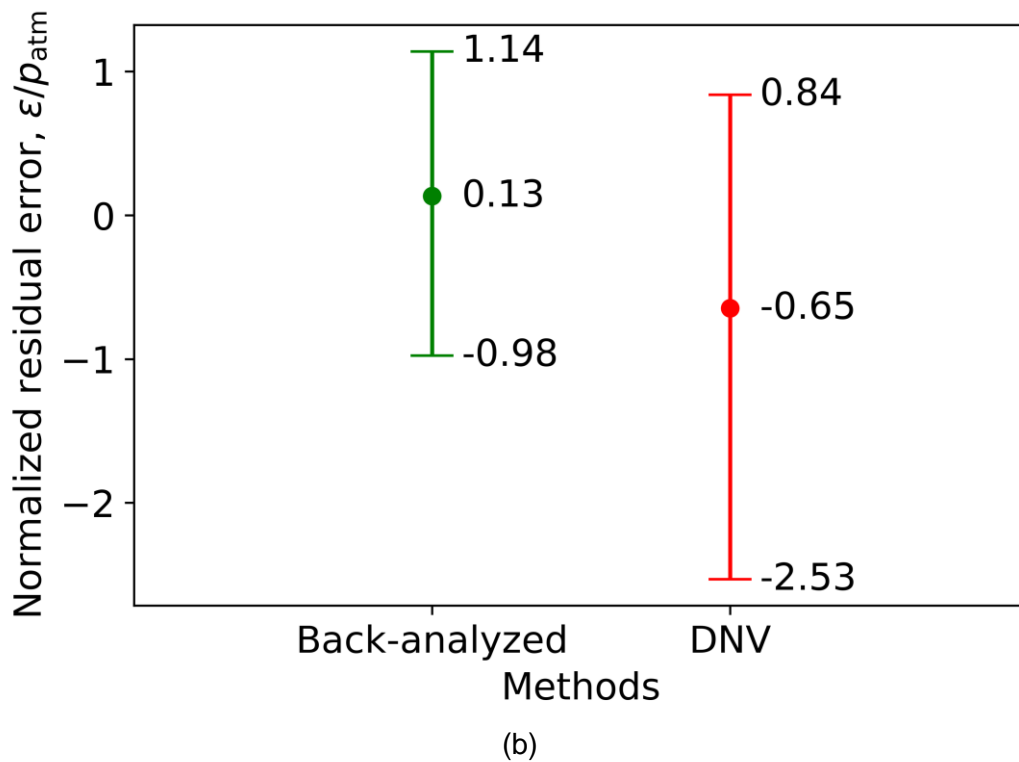
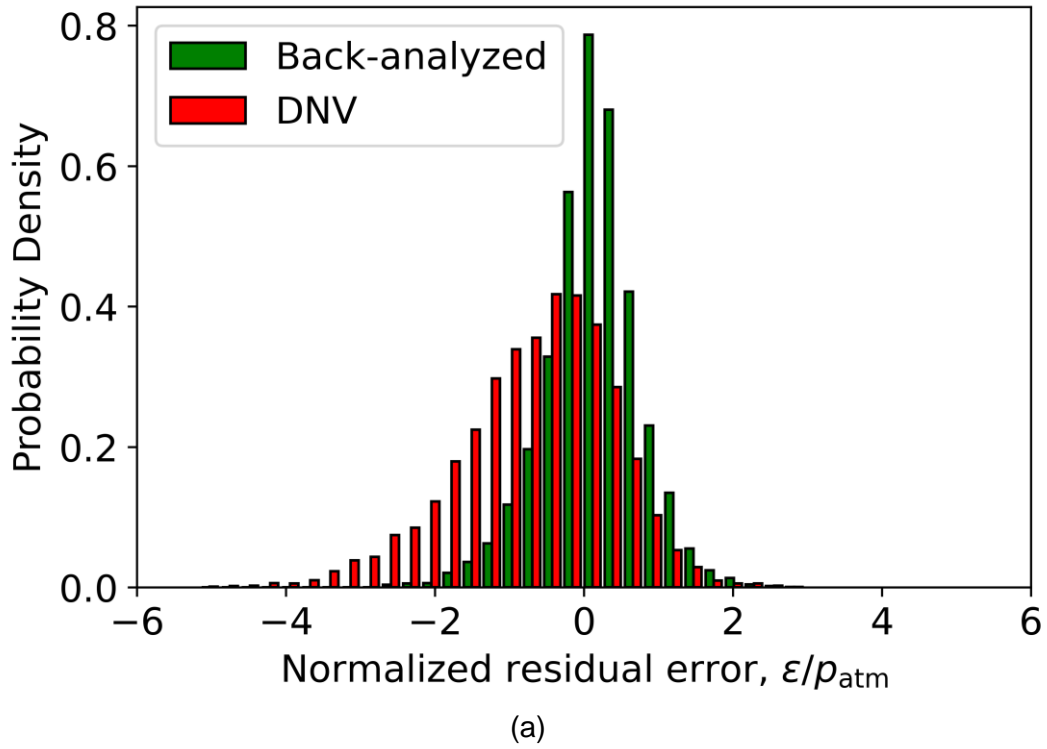


Figure 8. (a) Histogram of the residual errors of the calculations using the back-analyzed and DNV factors, relative to the measured values, for the training dataset; (b) Error bars of the residual errors. The circle marker represents the mean, while the end bars represent the 5th and 95th percentiles.

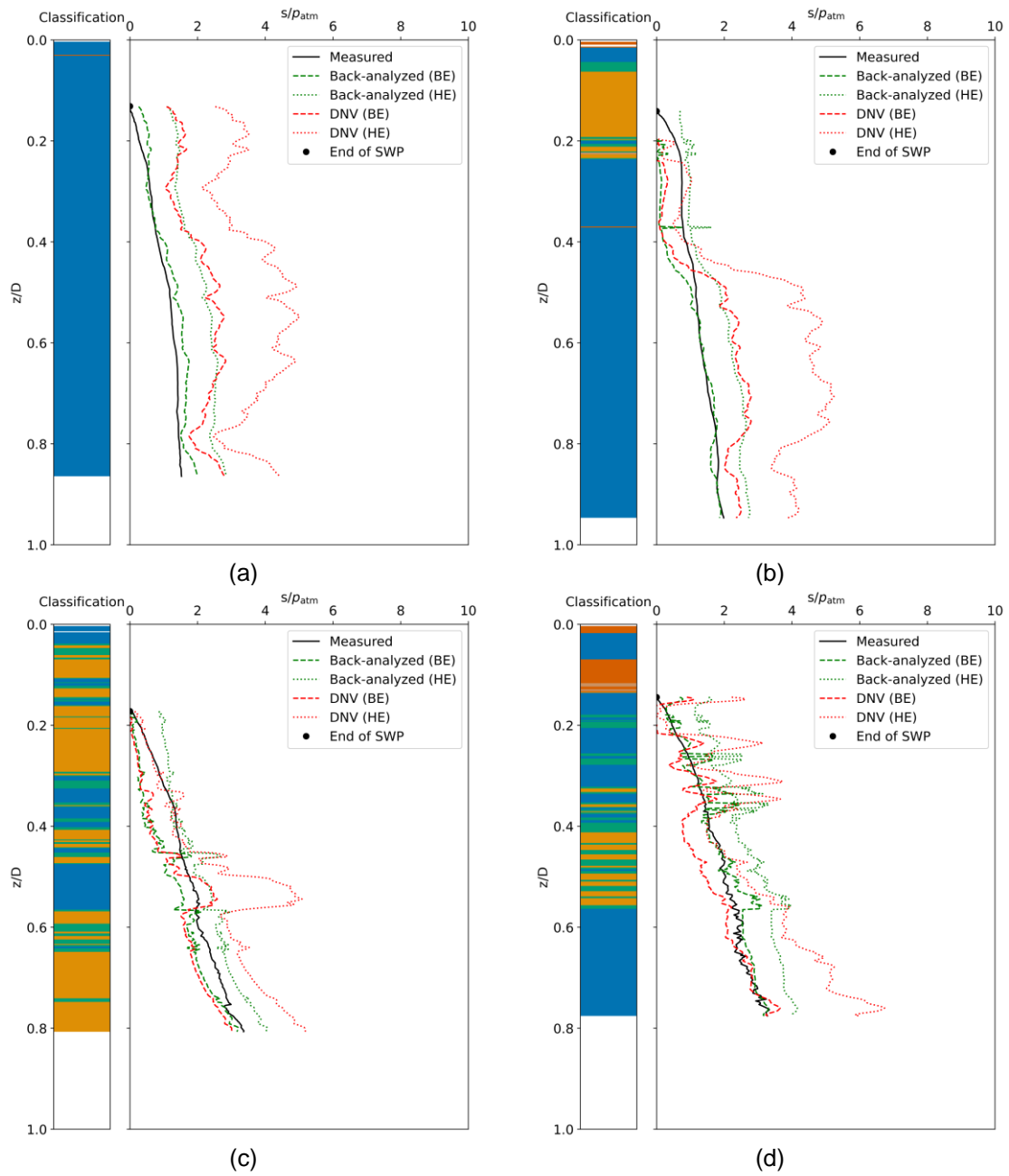
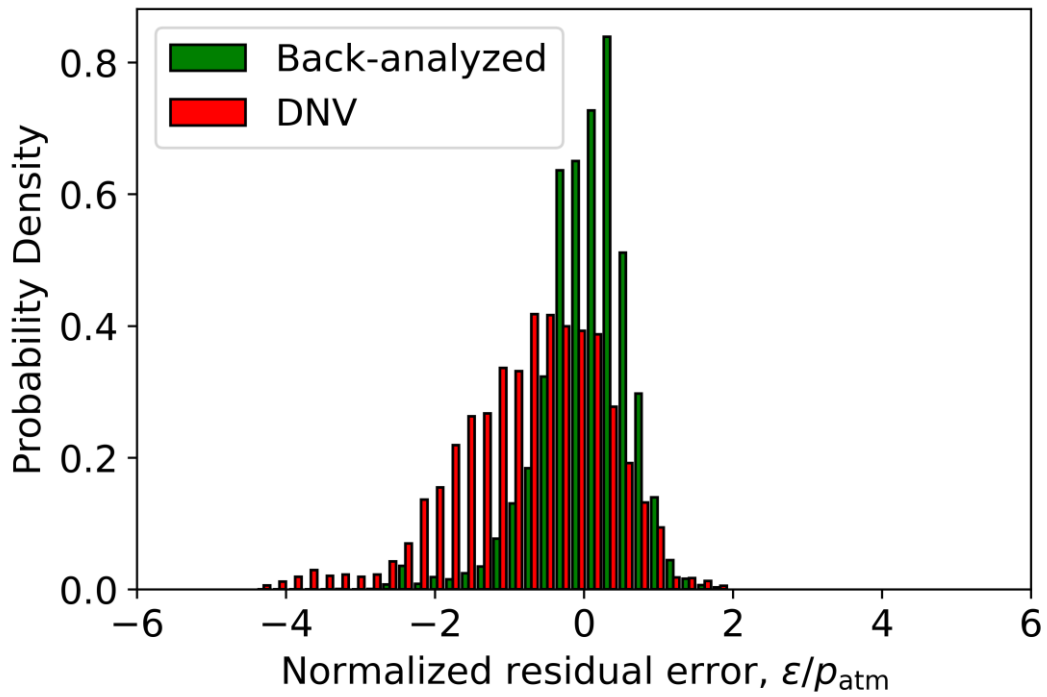
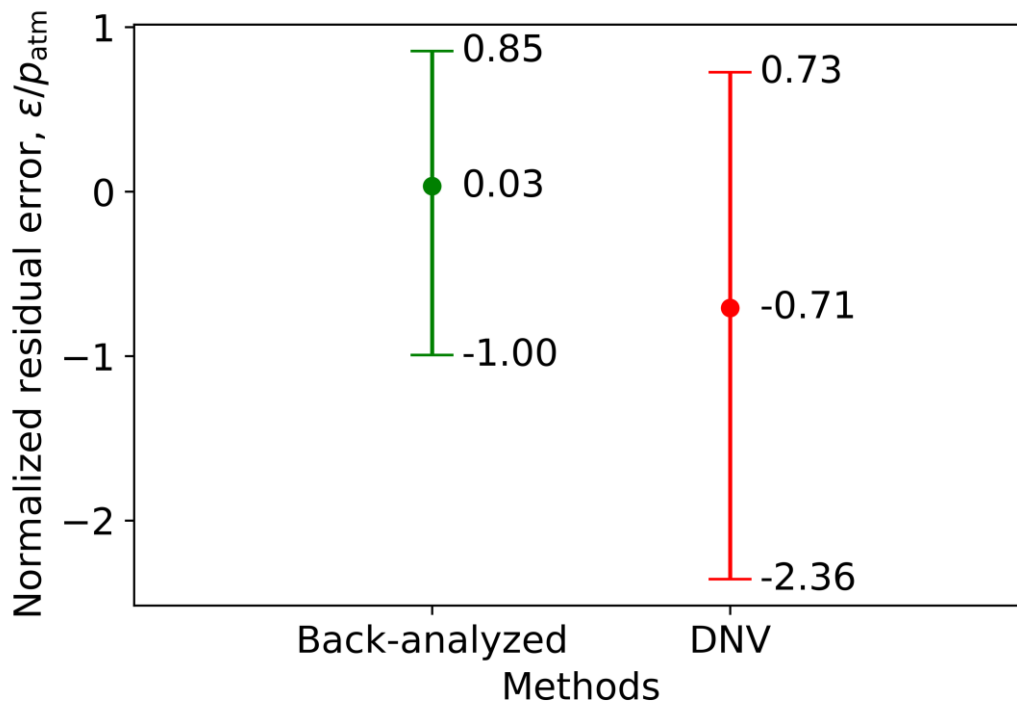


Figure 9. Comparison of required suction pressure vs penetration profiles for several locations in the training dataset, as calculated using the DNV and back-analyzed factors. Refer to Figure 3 for the color legend of the Robertson (2016) SBT categories.



(a)



(b)

Figure 10. (a) Histogram of the residual errors of the calculations using the back-analyzed and DNV factors, relative to the measured values, for the test dataset; (b) Error bars of the residual errors. The circle marker represents the mean, while the end bars represent the 5th and 95th percentiles.

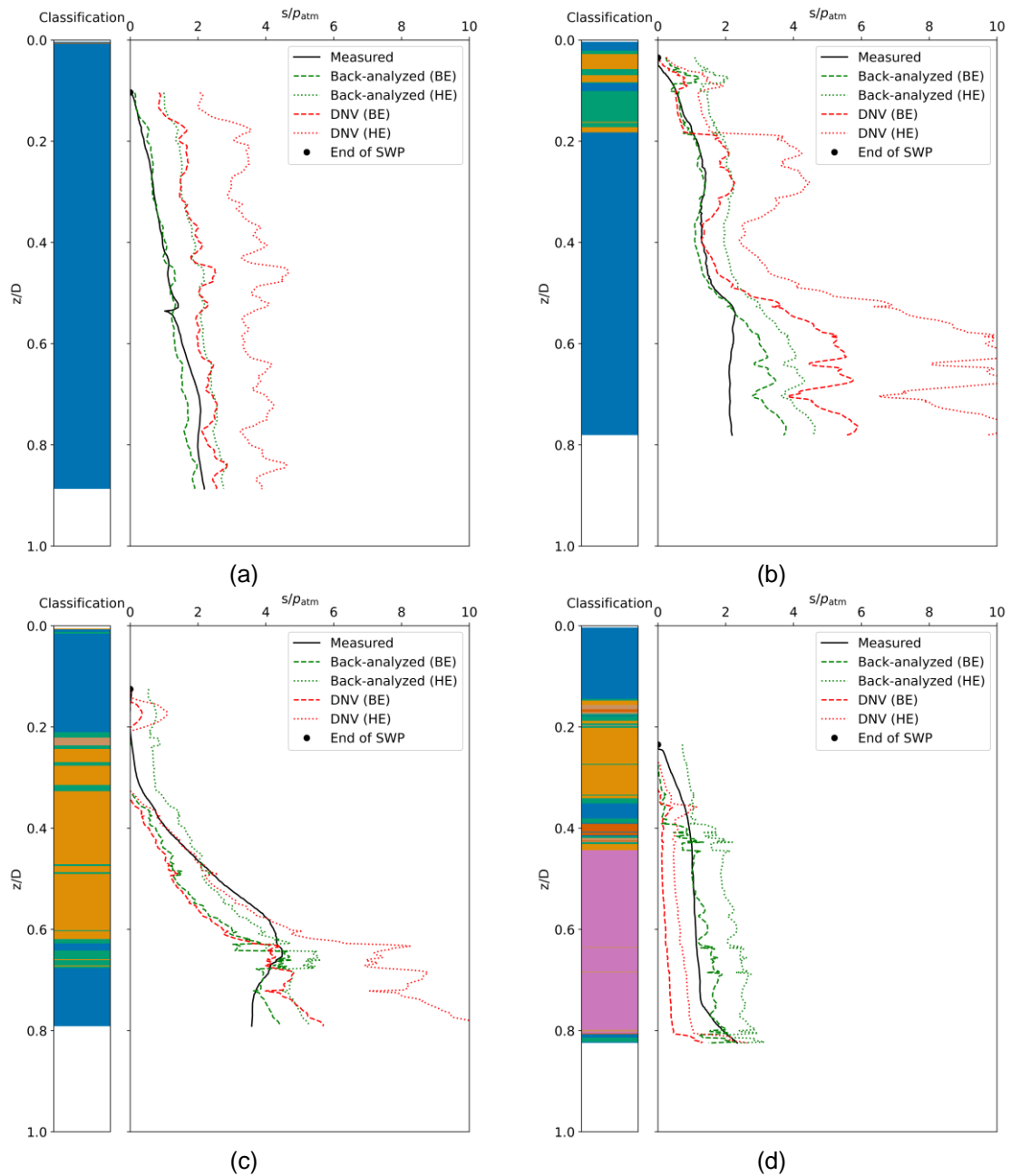


Figure 11. Comparison of required suction pressure vs penetration profiles for several locations in the test dataset, as calculated using the DNV and back-analyzed factors. Refer to Figure 3 for the color legend of the Robertson (2016) SBT categories.